

Implicit Deep Random Vortex Methods (iDRVM) for simulating incompressible flows in wall bounded domains

By V. Cherepanov*, S. W. Ertel†

Abstract

In this paper we introduce a novel Neural Networks-based approach for approximating solutions to the (2D) incompressible Navier–Stokes equations, which is an extension of so called Deep Random Vortex Methods (DRVM), that does not require the knowledge of the Biot–Savart kernel associated to the computational domain. Our algorithm uses a Neural Network (NN), that approximates the vorticity based on a loss function that uses a computationally efficient formulation of the Random Vortex Dynamics. The neural vorticity estimator is then combined with traditional numerical PDE-solvers, which can be considered as a final implicit linear layer of the network, for the Poisson equation to compute the velocity field. The main advantage of our method compared to the standard DRVM and other NN-based numerical algorithms is that it strictly enforces physical properties, such as incompressibility or (no slip) boundary conditions, which might be hard to guarantee otherwise. The approximation abilities of our algorithm, and its capability for incorporating measurement data, are validated by several numerical experiments.

Key words: incompressible fluid flow, no-slip boundary conditions, numerical simulation, random vortex method, Neural Networks, Deep Learning

MSC classifications: 76M35, 76M23, 60H30, 65C05, 68Q10.

1 Introduction

In recent years, the usage of Neural Networks (NNs) and deep learning techniques for numerical approximations of Partial Differential Equations (PDEs) has become an increasingly popular alternative to classical numerical solvers such as finite difference and finite element schemes. By now there exist many different approaches for NN-based PDE solvers, so that listing all of them is out of the scope of this introduction.

One of the most general NN-based numerical schemes is the Deep Galerkin Method (DGM) [30]. Similar to Physics-Informed Neural Networks (PINNs) (see e.g. [29]), the DGM directly incorporates the PDE into the loss function, which is usually chosen to be the L^2 -norm of the PDE residual w.r.t. some probability measure. Boundary conditions

*Mathematical Institute, University of Oxford, Oxford OX2 6GG. Email: vladislav.cherepanov@maths.ox.ac.uk

†Institut für Mathematik, Technische Universität Berlin, Straße des 17. Juni 136, 10623 Berlin, DE. Email: ertel@math.tu-berlin.de

and other properties of the solution of the PDE can be incorporated directly into the loss function by just adding the corresponding (weighted) residual terms.

A popular alternative are approaches based on stochastic representations of the PDE such as Feynman–Kac formulae [3] or Backward Stochastic Differential equations [15],[4]. While such methods are restricted to certain classes of second order PDEs, they provide an efficient numerical approximation scheme that can provably overcome the curse of dimensionality [14].

The main area of application for NN-based PDE solvers so far seems to be in high dimensional regimes where classical grid based schemes are too computationally expensive and therefore not viable. However even in low dimensional settings accurate approximations of certain PDEs can be prohibitively computationally expensive. In turbulent regimes this is for example the case for the (incompressible) Navier–Stokes equations

$$\begin{aligned} \partial_t u &= \nu \Delta_x u - (u \cdot \nabla_x) u - \nabla_x p + f & \text{on } D \\ \nabla_x \cdot u &= 0 & \text{on } D \\ u &= 0 & \text{on } \partial D, \end{aligned} \tag{1.1}$$

which describe the evolution of the velocity field u of some incompressible fluid and its pressure p . The parameter $\nu > 0$ denotes the viscosity of the fluid, f some external force and the domain D is typically two or three dimensional, i.e. $D \subseteq \mathbb{R}^2$ or $D \subseteq \mathbb{R}^3$. As usual Δ_x and ∇_x denote the (spatial) Laplacian and gradient respectively.

As direct numerical simulations of (1.1) based on classical solvers can require huge computation hours, NN-based techniques to design efficient approximation schemes have recently received increasing attention. While general NN-based PDE solvers like the aforementioned DGM can in principle also be applied to the Navier–Stokes equations (1.1), their special structure with the only implicitly determined pressure p makes the design of appropriate loss functions non trivial [22]. PINNs for Computational Fluid Dynamics (CFD) have been explored e.g. in [5],[16]. Other popular NN-based solvers make use of the specific structure of the Navier–Stokes equations. One very prominent approach hereby is to use NN-closures for Reynolds-averaged Navier-Stokes, see e.g. [25] and the references found therein.

An alternative probabilistic approach that has recently been proposed in [33] is the so called Deep Random Vortex Method (DRVM). It combines a stochastic representation of the Navier–Stokes equations by Random Vortex Dynamics, with a NN approximation u^θ of the velocity field u . The chosen loss function hereby controls the L^2 -distance between u^θ and u . While this method delivers an efficient approximation scheme, its scope is severely limited by the fact that it requires the explicit knowledge of the Biot–Savart kernel K associated to the domain D . In most applications this kernel will not be available. Also, even though the NN-approximation u^θ , might be reasonably close to u in L^2 , it can not be guaranteed that it (even approximately) respects the homogeneous boundary conditions (see also Section 3). This is an issue that is shared by many NN-based approaches, as appropriately incorporating such constraints into the NN can be difficult, as it would either require an adaptation of the architecture (final activation layer) or an adaptation of the loss function through Lagrange multipliers. Designing such adaptations efficiently for general computational domains however is a highly challenging task.

To overcome this problem we therefore derive a novel variant of DRVNs that combines a NN-based approximation of the vorticity with traditional numerical PDE solvers, acting as a final implicit layer of the network, to compute the fluid velocity from a Poisson equation. In each training cycle of the network ω^θ we first optimize the weights θ of the

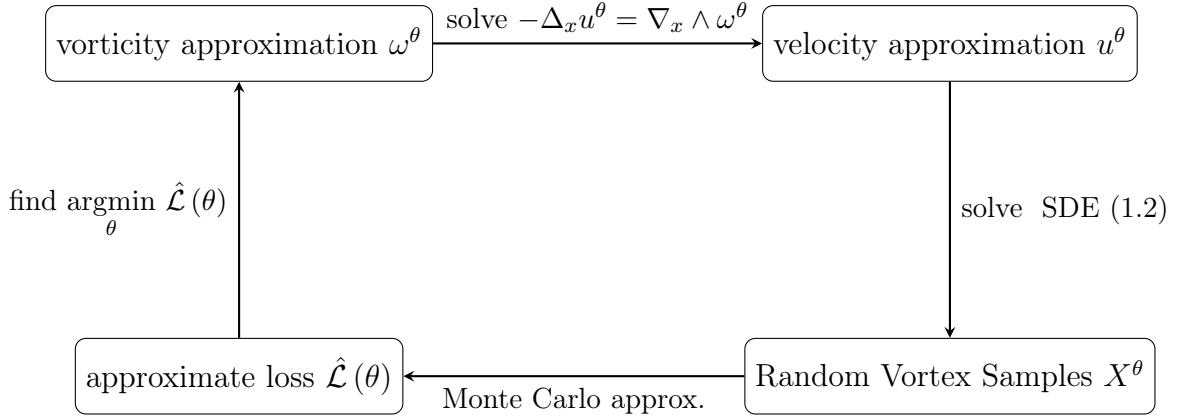


Figure 1.1: Training cycle of our NN-based algorithm. To simulate the Navier–Stokes equations, these training cycles are repeated several times until ω^θ can be expected to sufficiently approximate ω .

NN according to a Monte Carlo approximation $\hat{\mathcal{L}}(\theta)$ of a loss function $\mathcal{L}(\theta)$, which is equivalent to the L^2 -distance $\int_0^T \|\omega(\cdot, t) - \omega^\theta(\cdot, t)\|_{L^2(D)}^2 dt$ between the true vorticity $\omega := \nabla_x \wedge u$ and our NN-approximation ω^θ . Similar to the DRVM this loss function is based on a stochastic representation of the Navier–Stokes equations using Random Vortex Dynamics. Then we compute an approximation u^θ of the fluid velocity by (numerically) solving the Poisson equation $-\Delta_x u^\theta = \nabla_x \wedge \omega^\theta$, which is a consequence of the incompressibility of the fluid. With this approximate velocity u^θ at hand, we then generate samples from the diffusion process

$$dX_\xi^\theta(t) = u^\theta(X_\xi^\theta(t), t) dt + \sqrt{2\nu} dB_t, \quad X_\xi^\theta(0) = \xi, \quad (1.2)$$

which then in turn lets us compute an updated Monte Carlo approximation $\hat{\mathcal{L}}(\theta)$ of the loss function, and restart the training cycle (depicted in Flowchart 1.1, see also Algorithm 1 for pseudocode).

Note that this algorithm produces a NN-based numerical solver for the Navier–Stokes equation in which the NN is trained on artificially generated data. However, as discussed in Section 6, one can easily adapt our method to incorporate (real world) measurement data by adapting the loss function $\hat{\mathcal{L}}(\theta)$ and thus create a PINN.

This approach has several advantages:

- As traditional PDE solvers usually strictly enforce the homogeneous Dirichlet conditions of u , this alleviates the previously discussed issue of incorporating the boundary conditions into the training of the network.
- It allows the usage of state of the art numerical solvers for elliptic PDEs as a black box for the computation of the velocity from neural vorticity approximations. Therefore simulations in domains D with complex boundary geometry are possible with our approach. In particular, unlike the DRVM of [33], our method does not require the explicit knowledge of the Biot–Savart kernel, which for most domains D will not be available.
- Solving the Poisson equation has a regularizing effect and thus one can expect that this approach gives approximations in the more regular $H^1(D)$ -Sobolev norm .

In the following sections we describe our algorithm in detail and show its effectiveness for simulating incompressible fluid flows through several numerical experiments. In Section 2 we briefly introduce the so called Random Vortex Dynamics, a stochastic representation of the Navier–Stokes equation, which are the basis for our approximation scheme. In Section 3 we show how a loss function for neural vorticity approximations can be constructed from these Random Vortex Dynamics. In this section we also compare our approach of approximating the vorticity with direct approximations of the velocity, which were considered in [33]. In Section 4 we specify our proposed algorithm in detail, including a description in pseudo code. Furthermore in Section 5 and Section 6 we discuss how the proposed algorithm can be adapted easily for periodic boundary conditions and for incorporating (real world) measurement data. Finally, in Section 7, we show the effectiveness of our method through several numerical experiments.

2 Vorticity and its random vortex representation

Just as in [33], a key component of our Neural PDE-solver are stochastic representations of the vorticity of the Navier–Stokes equation. For the sake of (notational) simplicity we shall assume throughout this paper that we are investigating a two dimensional flow, i.e. $D \subseteq \mathbb{R}^2$, however we note that by using recently found 3D Random Vortex Dynamics [27],[28], our algorithm can be generalized to domains in \mathbb{R}^3 . For two dimensional velocity fields u , their vorticity ω is a scalar field, defined by $\omega := \nabla_x \wedge u := \partial_{x_1} u^2 - \partial_{x_2} u^1$. Using the Navier–Stokes equations (1.1) and elementary vector calculus, one shows that ω satisfies the vorticity equation [24]

$$\partial_t \omega = \nu \Delta_x \omega - (u \cdot \nabla_x) \omega + g \quad \text{on } D, \quad (2.1)$$

which is a one-dimensional Fokker–Planck equation with drift u and inhomogeneity $g := \nabla_x \wedge f$. Note that the boundary conditions of ω are only known implicitly through the velocity u .

Notice that while u is only determined within the domain $D \subseteq \mathbb{R}^2$, due to the boundary conditions $u(x, t) = 0$ for $x \in \partial D, t \geq 0$, we can trivially extend u on the full plane by setting $u(x, t) = 0$ for any $x \notin D, t \geq 0$. In particular if $u(\cdot, t) \in H^1(D)$ is a Sobolev function of order 1, then it is easy to check that the same is true for the extension on the full plane, i.e. $u(\cdot, t) \in H^1(\mathbb{R}^2)$.

With this extension we can define the Random Vortex Dynamics X , which is the family of diffusion processes, defined by the stochastic differential equations (SDEs)

$$\begin{aligned} dX_{\eta;\tau}(t) &= u(X_{\eta;\tau}(t), t) dt + \sqrt{2\nu} dB_t \quad \text{for } t \geq \tau, \\ X_{\eta;\tau}(\tau) &= \eta, \end{aligned} \quad (2.2)$$

for some standard 2D Brownian motion $(B_t)_{t \geq 0}$. In the following we will often leave out the starting time parameter τ , when $\tau = 0$, i.e. we set $X_\eta := X_{\eta;0}$ for any $\eta \in \mathbb{R}^2$.

Their transition probability densities

$$p_u(\tau, \eta, t, x) := \mathbb{P}(X_{\eta;\tau}(t) \in dx), \quad (2.3)$$

are fundamental solutions of the vorticity equation (2.1). But only on the full plane $D = \mathbb{R}^2$ they also coincide with the Green’s function (i.e. the integral kernel through

which the solutions to (2.1) can be represented via convolution), due to the absence of boundary conditions.

With these definitions in mind one can derive a representation of the vorticity ω by the family of diffusion processes X . To simplify the exposition, we assume that the domain is the upper-half plane $\{x \in \mathbb{R}^2 : x_2 > 0\}$, however the representations presented below are valid for more general domains (see [8]).

Let us denote by ζ the values of the vorticity at the boundary, i.e. $\zeta(x_1, t) := \omega((x_1, 0), t)$ for $x_1 \in \mathbb{R}$. Then we introduce a perturbation of the vorticity as follows. For a smooth cut-off function $\varphi : [0, \infty) \rightarrow [0, 1]$, such that $\varphi(r) = 1$ for $r \in [0, 1/2]$ and $\varphi(r) = 0$ for $r \geq 1$, define the perturbation $\sigma_\varepsilon(x, t) := \varphi(x_2/\varepsilon)\zeta(x_1, t)$ for some $\varepsilon > 0$, and let

$$\omega_\varepsilon(x, t) = \omega(x, t) - \sigma_\varepsilon(x, t). \quad (2.4)$$

Then

$$\partial_t \omega_\varepsilon = \nu \Delta_x \omega_\varepsilon - (u \cdot \nabla_x) \omega_\varepsilon + g_\varepsilon,$$

with $\omega_\varepsilon|_{\partial D} = 0$, and the perturbed external vorticity g_ε is given by

$$g_\varepsilon = g - \partial_t \sigma_\varepsilon - (u \cdot \nabla_x) \sigma_\varepsilon + \nu \Delta_x \sigma_\varepsilon. \quad (2.5)$$

As shown in [8], the perturbed vorticity satisfies the following representation

$$\begin{aligned} \omega_\varepsilon(\xi, t) &= \int_D \mathbb{E}^{\eta \rightarrow \xi} [1_{\{t < \tau_t(X_\eta)\}}] \omega_\varepsilon(\eta, 0) p_u(0, \eta, t, \xi) d\eta \\ &\quad + \int_0^t \int_D \mathbb{E}^{\eta \rightarrow \xi} [1_{\{t-s < \tau_t(X_\eta)\}}] g_\varepsilon(X_\eta(s), s) p_u(0, \eta, t, \xi) d\eta ds, \end{aligned} \quad (2.6)$$

where τ_t is the last hitting time of the boundary ∂D before time t , and $\mathbb{E}^{\eta \rightarrow \xi}$ denotes the expectation conditioned on $X_\eta(t) = \xi$. Then, given any (appropriate) test function ϕ , this provides the weak formulation of the vorticity in the limit as $\varepsilon \rightarrow 0$

$$\begin{aligned} \int_D \omega(x, t) \phi(x) dx &= \int_D \mathbb{E} [\phi(X_\eta(t)) 1_{\{t < \tau_t(X_\eta)\}}] \omega(\eta, 0) d\eta \\ &\quad + \lim_{\varepsilon \rightarrow 0} \int_D \mathbb{E} \left[\phi(X_\eta(t)) \int_0^t g_\varepsilon(X_\eta(s), s) 1_{\{t-s < \tau_t(X_\eta)\}} ds \right] d\eta. \end{aligned} \quad (2.7)$$

In the perturbation of external vorticity $g_\varepsilon - g$, the only term that contributes to the limit is $\rho_\varepsilon(x, t) := \nu \frac{\partial^2}{\partial x_2^2} \sigma_\varepsilon(x, t) = \frac{\nu}{\varepsilon^2} \varphi''(x_2/\varepsilon) \zeta(x_1, t)$. In general, its limit is represented as an integral with $\frac{\partial}{\partial n} p^D(0, \eta, t, \xi)$, where $\frac{\partial}{\partial n}$ is the normal derivative at the boundary in η variables — one writes it as the following boundary integral

$$\nu \int_0^t \int_{\partial D} \frac{\partial}{\partial n} \mathbb{E} [\phi(X_\eta(t)) 1_{\{t-s < \tau_t(X_\eta)\}}] \zeta(\eta, s) d\eta ds. \quad (2.8)$$

In practice, however, we approximate the term computing for some small ε the following

$$\Omega_\varepsilon(\eta, t) := \omega(\eta, 0) 1_{\{t < \tau_t(X_\eta)\}} + \int_0^t (g(X_\eta(s), s) + \rho_\varepsilon(X_\eta(s), s)) 1_{\{t-s < \tau_t(X_\eta)\}} ds \quad (2.9)$$

and writing

$$\int_D \omega(x, t) \phi(x) dx \approx \int_D \mathbb{E} [\Omega_\varepsilon(\eta, t) \phi(X_\eta(t))] d\eta. \quad (2.10)$$

In the following, we will often omit the parameter ε in Ω_ε to ease the notation.

Thus, given samples X^i , $i = 1, \dots, N$ of the diffusion process (2.2), one can approximate the integration of the vorticity ω against test functions ϕ . However to generate such samples one would need to know the velocity u a priori. Instead one uses approximate samples. To this end one first rewrites the velocity u in (2.2) as an integral of the vorticity ω , turning (2.2) into a closed system of McKean–Vlasov equations. Then one uses a mean-field interacting particle system to generate approximate samples. To write (2.1) into a closed form, one can use that u is divergence free, to show that

$$-\Delta_x u = \nabla_x \wedge \omega := \begin{pmatrix} \partial_{x_2} \omega \\ -\partial_{x_1} \omega \end{pmatrix} \quad \text{on } D. \quad (2.11)$$

Let now $\mathcal{G} : D \times D \rightarrow \mathbb{R}$ be the Green’s function of $(-\Delta_x)$ on D , then the Biot–Savart kernel $K : D \times D \rightarrow \mathbb{R}$ is defined by

$$K(x, y) := \nabla_x \wedge \mathcal{G} := \begin{pmatrix} \partial_{x_2} \mathcal{G}(x, y) \\ -\partial_{x_1} \mathcal{G}(x, y) \end{pmatrix}. \quad (2.12)$$

Combining the Poisson equation (2.11) with the definition of the Biot–Savart kernel implies the so called Biot–Savart law

$$u(y, t) = \int_D K(x, y) \omega(x, t) dx, \quad (2.13)$$

which in turn can be combined with the stochastic representation (2.7), to rewrite the velocity u into

$$\begin{aligned} u(y, t) &= \int_D \mathbb{E} [K(X_\eta(t), y) 1_{\{t < \tau_t(X_\eta)\}}] \omega(\eta, 0) d\eta \\ &+ \lim_{\varepsilon \rightarrow 0} \int_D \mathbb{E} \left[K(X_\eta(t), y) \int_0^t g_\varepsilon(X_\eta(s), s) 1_{\{t-s < \tau_t(X_\eta)\}} ds \right] d\eta. \end{aligned} \quad (2.14)$$

Thus the Random Vortex Dynamics (2.2) can be rewritten into closed form as a flow of McKean–Vlasov equations. As usual these McKean–Vlasov equations can be approximated by a system of interacting (ordinary) SDEs, leading to a Monte–Carlo approximation of the velocity, called Random Vortex Methods (RVM). In the simplest setting, namely $D = \mathbb{R}^2$, $g = 0$, this is a classical method in Computational Fluid Dynamics, first investigated by Chorin [9] in the 1970s, see also e.g. [10],[13],[23]. Recently efficient variants of the RVM for some domains involving a boundary and an external force have been derived based on the stochastic representation (2.7) above, see [6],[8],[27].

Nevertheless vanilla Monte Carlo simulations can be inefficient and for general domains designing accurate numerical approximations based on the stochastic representation (2.7) above can be challenging, in particular because the Biot–Savart kernel will usually be unknown. Therefore, similar to the DRVM from [33], we propose a NN-based alternative to the standard Monte Carlo approximation of (2.7) and thus also of u . The usage of NNs in our algorithm and its comparison to the previously derived DRVM, is discussed in the next section.

Remark 1. *Note that for certain settings formula (2.14) can be simplified significantly. E.g. if the velocity evolves on the full plane, i.e. $D = \mathbb{R}^2$, and if no external force influences the vorticity, i.e. $g = 0$, then (2.14) can be simplified into*

$$u(y, t) = \int_D \mathbb{E} [K(X_\eta(t), y)] \omega(\eta, 0) d\eta, \quad (2.15)$$

where the Biot–Savart kernel is given by $K(x, y) = \frac{1}{2\pi} \frac{(x-y)^\perp}{\|x-y\|^2}$. This was the setting considered by Chorin [9] and other classical works on RVMs. Identity (2.15) also holds true if the domain D is the two dimensional torus, the homogenous Dirichlet boundary conditions are replaced by periodic boundary conditions and K is the Biot–Savart kernel on the torus. However for general domains $D \subseteq \mathbb{R}^2$, the simplified representation formula (2.15) can not be expected to hold.

3 Approximating velocity vs. vorticity

The DRVM, proposed by [33], used NNs to approximate the velocity directly. These networks are trained to minimize the L^2 -distance to the true velocity u , which is approximated by using Monte Carlo approximations based on the formula (2.15) in Section 2. More precisely, consider a NN (or, more generally, other function approximators) $u^\theta : \mathbb{R}^2 \times [0, T] \rightarrow \mathbb{R}^2$, where θ denotes the trainable parameters/weights. To construct the loss function denote by X^θ the family of diffusions

$$\begin{aligned} dX_\eta^\theta(t) &= u^\theta(X_\eta^\theta(t), t) dt + \sqrt{2\nu} dB_t \quad \text{for } t \geq 0, \\ X_\eta^\theta(0) &= \eta. \end{aligned} \tag{3.1}$$

With this notation, the loss function \mathcal{L} used for training the NN was constructed from (2.15) as

$$\mathcal{L}(\theta) := \int_0^T \int_D \left\| u^\theta(y, t) - \int_D \mathbb{E} [K(X_\eta^\theta(t), y)] \omega(\eta, 0) d\eta \right\|^2 dy dt. \tag{3.2}$$

Remark 2. Note that while in the loss function (3.2), only the evaluations of u^θ inside the domain D appear, the SDE (3.1) requires u^θ to be defined on the whole plane \mathbb{R}^2 .

As mentioned in Remark 1, approximations based on this loss function (3.2) can only be expected to result in good approximations of u in certain settings that do not involve boundaries with no slip conditions, e.g. when the domain D is the full plane \mathbb{R}^2 or the torus, as more general domains would require adaptations based on the more complex representation formula (2.14). However, even with such adaptations, this approach requires knowledge of the Biot–Savart kernel K associated to the computational domain D , which is not known explicitly for most domains D .

Furthermore, even in the few cases where K is known explicitly and the representation formula (2.15) holds, the minimization of the loss function (3.2) can at best be expected to result in an approximation of the true velocity with respect to the L^2 -norm. However L^2 -convergence can of course not guarantee that the approximations capture the right behaviour of the fluid near the boundary, since the trace $u^\theta|_{\partial D \times [0, T]}$ is of course not continuous with respect to the L^2 -norm (see Remark 3 for a very elementary counterexample). This is in particular problematic for many engineering applications, where one is often primarily interested in the behaviour of the fluid near the boundary in order to compute boundary stress.

Remark 3. For any function $u : \mathbb{R}^2 \rightarrow \mathbb{R}$ one can easily construct a sequence of perturbations $(u^\epsilon)_{\epsilon > 0}$, such that $\|u - u^\epsilon\|_{L^2(D)} \xrightarrow{\epsilon \rightarrow 0} 0$, but $\inf_{x \in \partial D} \|u(x) - u^\epsilon(x)\| \xrightarrow{\epsilon \rightarrow 0} +\infty$. To construct such perturbations, denote the ϵ -neighborhood around the boundary ∂D by

$U_\epsilon(\partial D)$, denote its Lebesgue measure by $\text{Leb}(U_\epsilon(\partial D))$ and let $\phi_\epsilon : \mathbb{R}^2 \rightarrow \mathbb{R}$ be a smooth function with

$$\mathbb{1}_{U_{\epsilon/2}(\partial D)} \leq \phi_\epsilon \leq \mathbb{1}_{U_\epsilon(\partial D)}.$$

Then for $u_\epsilon(x) := u(x) + \frac{\phi_\epsilon(x)}{\text{Leb}(U_\epsilon(\partial D))^{1/4}}$, $x \in \mathbb{R}^2$, we have

$$\begin{aligned} \|u_\epsilon(\cdot, t) - u(\cdot, t)\|_{L^2(D)}^2 &\leq \text{Leb}(U_\epsilon(\partial D))^{1/2} \xrightarrow{\epsilon \rightarrow 0} 0 \\ \inf_{x \in \partial D} \|u_\epsilon(x) - u(x)\|^2 &= \frac{1}{\text{Leb}(U_\epsilon(\partial D))^{1/2}} \xrightarrow{\epsilon \rightarrow 0} +\infty. \end{aligned}$$

One simple way to address this issue would be an incorporation of the boundary data into the loss function via Lagrange multipliers, similar to what is done in DGM. However, this may negatively impact the training of the network and may result in a worse performance. Another alternative would be to adapt the final (activation) layer of the network to enforce that the boundary conditions are satisfied, however for general domains such adapted activation functions may be difficult to find and may also negatively impact the performance of the network.

A simple alternative, which we investigate in this paper, is that a NN ω^θ is only trained to approximate the vorticity ω . The velocity is then approximated by the output u^θ of standard elliptic PDE solvers via the Poisson equation (2.11). Note that the continuity of the Poisson equation (2.11) with respect to the right hand side¹ implies

$$\|u(\cdot, t) - u^\theta(\cdot, t)\|_{H^1(D)} \leq \sqrt{1 + C_P^2} \|\omega(\cdot, t) - \omega^\theta(\cdot, t)\|_{L^2(D)} \quad (3.3)$$

where C_P is the Poincaré constant of the domain D . Therefore, assuming that at any time $t \geq 0$ the NN $\omega^\theta(\cdot, t)$ approximates the true vorticity $\omega(\cdot, t)$ in $L^2(D)$, as well as that the chosen numerical PDE solver returns accurate approximations w.r.t. the $H^1(D)$ -norm, one can thus expect that with this approach u^θ approximates u in $H^1(D)$. In particular, since the restriction to the boundary

$$\cdot|_{\partial D} : H^1(D) \rightarrow L^2(\partial D),$$

is a bounded linear operator on $H^1(D)$, one would thus expect that the approximation captures the correct behaviour of the true velocity field u near the boundary.

To derive a loss function for our NN ω^θ , we use the stochastic representation (2.7) of the vorticity ω . Note that (2.7) only gives us a weak representation in the sense that it only describes the integration of ω against testfunctions. However, when using gradient-based optimization algorithms, this is enough for training the NN ω^θ to minimize an L^2 -loss, as by completing the square, we have

$$\begin{aligned} \|\omega^\theta - \omega\|_{D \times [0, T]}^2 &= \int_0^T \int_D |\omega^\theta(x, t) - \omega(x, t)|^2 dx dt \\ &= \int_0^T \int_D |\omega^\theta(x, t)|^2 dx dt - 2 \int_0^T \int_D \omega^\theta(x, t) \omega(x, t) dx dt + \int_0^T \int_D |\omega(x, t)|^2 dx dt. \end{aligned}$$

¹A standard result in PDE theory, see e.g. [11].

Note that the last integral is constant w.r.t. the parameters/weights θ . Thus, gradient descent algorithms (w.r.t. the parameters θ) applied to

$$\int_0^T \int_D |\omega^\theta(x, t)|^2 dx dt - 2 \int_0^T \int_D \omega^\theta(x, t) \omega(x, t) dx dt, \quad (3.4)$$

also minimize the L^2 -loss $\|\omega^\theta - \omega\|_{D \times [0, T]}^2$.

Using the approximate form (2.10) for the stochastic representation (2.7), we can rewrite (3.4) into

$$\int_0^T \int_D |\omega^\theta(\eta, t)|^2 d\eta dt - 2 \int_0^T \int_D \mathbb{E} [\Omega(\eta, t) \omega^\theta(X_\eta(t), t)] d\eta dt \quad (3.5)$$

However the diffusion process X is unknown, so computing (3.5) exactly is not possible. Instead we use the Poisson equation (2.11) to define a velocity approximation u^θ , based on the NN ω^θ . Thus define u^θ to be the unique solution of the Poisson equation with homogeneous Dirichlet boundary conditions

$$\begin{aligned} -\Delta_x u^\theta &= \nabla_x \wedge \omega^\theta \quad \text{on } D \\ u^\theta &= 0 \quad \text{on } \partial D. \end{aligned} \quad (3.6)$$

Outside the domain D set $u^\theta(x, t) = 0$, $x \notin D$, $t \geq 0$ and define the diffusion processes X^θ just as in (3.1). This in turn lets us define the loss function \mathcal{L} by

$$\mathcal{L}(\theta) := \int_0^T \int_D |\omega^\theta(\eta, t)|^2 d\eta dt - 2 \int_0^T \int_D \mathbb{E} [\Omega(\eta, t) \omega^\theta(X_\eta^\theta(t))] d\eta dt. \quad (3.7)$$

Remark 4. Note that while only ω^θ is a traditional (deep) NN and u^θ is obtained through the Poisson equation (3.6), one can also view u^θ as a NN with a final convolutional layer given by a convolution with the Biot–Savart kernel $u^\theta = K \circledast \omega^\theta$. However as the kernel K is usually not explicitly known one should thus rather view u^θ as a NN with a final linear, implicit layer, which in our case is determined by the Poisson equation (3.6). Such implicit layers have recently received increasing attention in the Machine Learning community, e.g. as part of Deep Equilibrium Models [2], where they are usually not given through differential equations, but rather by root finding problems of the form $F(u^\theta, \omega^\theta) = 0$.

4 Numerical algorithm

With the general loss function given in (3.7), we can describe the approximate loss $\hat{\mathcal{L}}$ that is used in simulations by first discretising the time and space integrals

$$\hat{\mathcal{L}}(\theta) \approx \sum_{k=0}^{N_{\text{steps}}} \left(\sum_i \omega^\theta(\eta^i, t_k)^2 \Delta\eta^i - 2 \sum_i \mathbb{E} [\Omega(\eta^i, t_k) \omega^\theta(X_{\eta^i}(t_k), t_k)] \Delta\eta^i \right) \Delta t_k, \quad (4.1)$$

and since in practice we compute the approximation ω^θ at each fixed time t_k , it is sufficient to consider

$$\hat{\mathcal{L}}(\theta, t_k) := \sum_i (\omega^\theta(\eta^i, t_k)^2 - 2 \mathbb{E} [\Omega(\eta^i, t_k) \omega^\theta(X_{\eta^i}(t_k), t_k)]) \Delta\eta^i \quad (4.2)$$

for the loss function at each step. In the above discretization, we used a finite set of lattice points $\eta^i \in D$, $i = 1, \dots, N$ with corresponding mesh sizes $\Delta\eta^i$ at each point.

Notice also that the discretized loss (4.2) has expectations with respect to stochastic processes X . One way to approximate them is to simulate independent copies of X and replace the expectations with averages. Another common way in Random Vortex methods is to run the processes X with independent Brownian motions corresponding to each site η^i and omit the expectations. In the algorithm we describe below, the second approach is adopted.

With the loss function we discussed above, we can state the following algorithm for our system. For lattice points $\eta^i \in D$, $i = 1, \dots, N$, initialize $X^i(0) = X_{\eta^i}(0)$ and $\Omega^i(0) = \Omega(\eta^i, 0)$. Then the system is updated with the following typical step:

1. With the current values of $\Omega^i(t)$ and the processes $X^i(t)$, find the minimizer $\hat{\theta}$ of $\hat{\mathcal{L}}(\cdot, t)$ in (4.2) and set

$$\hat{\omega}(\cdot, t) := \omega^{\hat{\theta}}(\cdot, t),$$

— note that we minimize the loss over parameters for a class of NNs, however, any suitable class of function approximators \mathcal{F} can be considered here.

2. Compute the velocity approximation from (2.11) with $\hat{\omega}$, i.e. \hat{u} is the numerical solution to

$$\Delta_x \hat{u} = -\nabla_x \wedge \hat{\omega},$$

which is computed through an applicable numerical solver, e.g. Finite Elements Methods, Finite Difference Schemes, Monte Carlo Methods (like Walk-on-spheres) or, when the kernel is known explicitly, discretisations of the Biot–Savart law (2.13).

3. Update the processes X^i by

$$X^i(t + \Delta t) = X^i(t) + \hat{u}(X^i(t), t) \Delta t + \sqrt{2\nu} \Delta B^i$$

for N independent Brownian motions B^i , $i = 1, \dots, N$ and update the values of Ω^i by (2.9).

4. Return to step 1.

A more detailed version of the algorithm above is found below in pseudocode in Algorithm 1 which is optimized so that the computation complexity at each step is constant in time.

5 Periodic boundary conditions

While no slip conditions usually describe the physically correct behaviour of a fluid at the boundary, also considering other boundary conditions allows for more flexibility when designing numerical experiments. In particular periodic boundaries are of great relevance for benchmarking, because they allow to consider flows in compact domains without restricting the motion of the fluid. In this case the computational domain D is often chosen to be a suitable subset of a rectangle $[0, L_x] \times [0, L_y]$, that may for example be of the form

$$D = [0, L_x] \times [0, L_y] \setminus O,$$

Algorithm 1 Random vortex algorithm.

Initialise: $X^i \leftarrow \eta^i$ for some lattice $\eta^i \in D$
Initialise: $\text{ind}^i \leftarrow 1$ ▷ indicators of X^i hitting the boundary
Initialise: $S^i \leftarrow (g(X^i, 0) + \rho_\varepsilon(X^i, 0))\Delta t$
Initialise: $\Omega^i \leftarrow \omega(X^i, 0) + S^i$
for $k \leftarrow 0$ to N_{steps} **do**
 Find: $\hat{\omega} = \omega^{\hat{\theta}}(\cdot, t_k)$, with $\hat{\theta} \leftarrow \text{argmin}_\theta \hat{\mathcal{L}}(\theta)$
 Solve: $\Delta_x \hat{u} = -\nabla_x \wedge \hat{\omega}$
 Compute: $X_{\text{upd}}^i \leftarrow \hat{u}(X^i, t_k)\Delta t + \sqrt{2\nu}\Delta B^i$
 Update: $X^i \leftarrow X^i + X_{\text{upd}}^i \cdot \text{ind}^i$
 if X^i crosses ∂D at x^i **then**
 Set: $X^i \leftarrow x^i$, $\text{ind}^i \leftarrow 0$, $S^i \leftarrow 0$
 end if
 Update: $S^i \leftarrow S^i + (g(X^i, t_k) + \rho_\varepsilon(X^i, t_k))\Delta t$
 Update: $\Omega^i = \omega(X^i, 0) \cdot \text{ind}^i + S^i$
end for

for some $O \subseteq (0, L_x) \times (0, L_y)$ representing an obstacle in the fluid flow. Periodicity of the flow may be enforced

1. only on the left side $\{0\} \times [0, L_y]$ and right side $\{L_x\} \times [0, L_y]$, i.e. $u((0, y)^T, t) = u((L_x, y), t)$ for $y \in [0, L_y]$
2. only on the bottom $[0, L_x] \times \{0\}$ and the top $[0, L_x] \times \{L_y\}$, i.e. $u((x, 0)^T, t) = u((x, L_y), t)$ for $x \in [0, L_x]$
3. on all sides $\partial([0, L_x] \times [0, L_y])$ of the torus, i.e. the conditions of both previous points 1 and 2 are satisfied.

On the other parts of the boundary ∂D , in particular on the boundary of the obstacle ∂O , one might then consider the usual no-slip conditions. In all three cases the stochastic representation formulas of Section 2 can be adapted rather easily for the periodic conditions by considering the random vortex dynamics (2.2) modulo the periodicity. In case 3, i.e. for of the fully periodic conditions of all sides of the box $\partial([0, L_x] \times [0, L_y])$, one considers the stochastic process $(X_\eta(t) \bmod (L_x, L_y)^T)_{t \geq 0}$ for X defined as in (2.2)². Extensions for periodicity conditions in only one direction follow similarly.

Remark 5. *As just described our Algorithm 1 can be extended easily to incorporate periodic boundary data. Our numerical experiments, described in Section 7, verify that it produces correct results without any adaptations to the loss function or the Neural Network architecture. However, while designing classes of Neural Networks that always satisfy given no-slip conditions is hard, one can easily design such architectures for periodic conditions by introducing a first periodic activation layer (periodic preprocessing).*

6 Incorporating measurement data/Data Assimilation

In recent years, partially due to the increasing availability of data, incorporating (real world) measurement data into numerical algorithms is an increasingly popular topic in

²This is equivalent to the periodic processing considered in [33, Equation (26)]

scientific computing. Especially in numerical weather prediction and adjacent fields such data driven approaches, usually referred to as Data Assimilation (see e.g. [12]), are often applied as they are capable of significantly improving the forecasting capabilities of numerical models. One popular approach for combining models with data is to minimize a cost function (hence called variational Data Assimilation) that incorporates both the misfit w.r.t. the model and the observation data.

Since our proposed Algorithm 1 is based on loss minimization, just as any other PINN, one can easily incorporate measurement data by simply adapting the loss function. To this end an additional term $\mathcal{R}(\theta)$, that measures data misfit, is added, i.e. instead of minimizing $\hat{\mathcal{L}}(\theta)$ (see (4.1)), one would minimize the adapted (empirical) loss function

$$\hat{\mathcal{L}}(\theta) := \hat{\mathcal{L}}(\theta) + \mathcal{R}(\theta),$$

for training the network ω^θ . The choice of \mathcal{R} will highly depend on the nature of the available data. If one is given actual measurements ω_k , $k = 1, \dots, K$ of the vorticity $\omega(x_k, t_k)$ at specific (spacetime) points $t_k \geq 0, x_k \in D$, then the most natural choice of \mathcal{R} is the simple L^2 -loss given by

$$\mathcal{R}(\theta) = \frac{1}{K} \sum_{k=1}^K \|\omega^\theta(x_k, t_k) - \omega_k\|^2. \quad (6.1)$$

However if one has only the fluid velocity u measurements and not its vorticity, this approach can still be adapted. In this case, when one is given velocity measurements u_k , $k = 1, \dots, K$ at specific spacetime points $t_k \geq 0, x_k \in D$, then a natural choice of \mathcal{R} is given by

$$\mathcal{R}(\theta) = \frac{1}{K} \sum_{k=1}^K \|u^\theta(x_k, t_k) - u_k\|^2,$$

where u^θ is the velocity approximation determined by the Poisson equation (3.6). While at first glance this may seem problematic for training the network, as the velocity approximation is only implicitly known through solving a PDE, the linearity of the Poisson equation (3.6) lets us compute gradients of u^θ , w.r.t. the weights/parameters θ in a simple manner. Let ∂_{θ_i} denote the derivative with respect to the i -th component of θ , then we note that $\partial_{\theta_i} u^\theta$ solves

$$\begin{aligned} -\Delta_x \partial_{\theta_i} u^\theta &= \nabla_x \wedge \partial_{\theta_i} \omega^\theta \quad \text{on } D \\ \partial_{\theta_i} u^\theta &= 0 \quad \text{on } \partial D, \end{aligned} \quad (6.2)$$

and we can thus compute gradients of u^θ w.r.t. the weights/parameters θ from the gradients of ω^θ by solving Poisson equations. In particular in situations where one has access to the Biot–Savart kernel K , which is a requirement for the DRVM of [33], one can directly represent $\partial_{\theta_i} u^\theta$ through the Biot–Savart law (2.13)

$$\partial_{\theta_i} u^\theta(x, t) = \int_D K(x, y) \partial_{\theta_i} \omega^\theta(y, t) dy. \quad (6.3)$$

7 Simulation results

Numerical Experiment 1 [Flow with prescribed boundary values]. In this example, we consider the fully bounded box domain $D = \{(x_1, x_2) \in \mathbb{R}^2 : 0 < x_1, x_2 < 1\}$ modelled with the lattice $\Lambda := \{(i_1 h, i_2 h) : 0 \leq i_1 \leq N, 0 \leq i_2 \leq N\}$. We take the following explicit solution

$$u(x_1, x_2) = \left(U_0^2 \frac{x_1}{\nu} e^{-U_0 \frac{x_2}{\nu}}, U_0 (e^{-U_0 \frac{x_2}{\nu}} - 1) \right) \quad (7.1)$$

restricted on the domain D . This implies that the vorticity $\omega(x_1, x_2, 0) = -U_0^3 \frac{x_1}{\nu} e^{-U_0 \frac{x_2}{\nu}}$ which we use to initialise the system. Notice that as the values of the velocity u are non-zero at the boundary ∂D which implies inhomogeneous boundary conditions in the Poisson equation (2.11), which we solve using finite element method discussed below.

For this experiment, we take the number $N = 50$ which results in 2601 points in total, and the mesh size $h = 1/N = 0.02$; the viscosity constant is taken $\nu = 0.01$ and the initial velocity constant $U_0 = 0.02$. We take the external force being identically zero which results in $g \equiv 0$. Thus, the external vorticity is generated only from the boundary vorticity ζ contributing to the term ρ_ε in (2.9). Here, we choose the boundary cutoff parameter $\varepsilon = 0.1$ with the cutoff function

$$\varphi(r) = 2(r - 0.5)^3 - \frac{3}{2}(r - 0.5) + \frac{1}{2}$$

for $r \in [0, 1]$, and zero otherwise.

The simulation is conducted for $N_{\text{steps}} = 100$ iterations with time steps $h_{\text{time}} = 0.01$ which gives the total time of $T = 1$, see Figure 7.2 for the plots of the approximated and true flows for times $t = 0.01, 0.5$ and 1.0 . In these figures, the streamlines are colored by the velocity magnitude while the background is colored by the vorticity value. We also include a heatmap of the absolute l2-error of our approximated solution in Figure 7.2, and plots of the learned and true vorticity in Figure 7.3.

Our experiment showed that our NN-based algorithm produces velocity/vorticity approximations that are close to the true solution. Particularly, one can see that error shown in Figure 7.2 is zero at the boundary which means that our algorithm enforces the correct inhomogeneous boundary conditions for the approximated velocity.

Another advantage of the proposed numerical algorithm is also outlined in Section 6 which allows for improving the quality of the results by adding additional penalisation for the approximation mismatching the measurement data. In order to demonstrate this in our experiment, we run the numerical scheme sampling at every timestep t points $z_i, i = 1, \dots, 2601$ independently and uniformly from D . We compute our "measurement data" as $\omega_i = \omega(z_i, t) + \sigma \varepsilon_i$ for ε_i being independent standard normal and $\sigma = 5 \times 10^{-3}$, where ω is the true vorticity found from (7.1). We use the values ω_i in the l2-loss (6.1) and add this term to our loss function (4.2). The relative l2-errors of the approximations found with the original loss and the assimilated data versions are given in Figure 7.4 which clearly demonstrates the improvement of adding data misfit penalisation.

Some further details of the algorithm implementation and the model training are discussed in this section below.

Numerical Experiment 2 [Taylor-Green vortex]. Consider D to be the torus which is represented by the periodized box $[0, 1] \times [0, 1]$ and we assume that the boundary $\partial D = \emptyset$. We take the lattice $\Lambda := \{(i_1 h, i_2 h) : 0 \leq i_1 \leq N, 0 \leq i_2 \leq N\}$ as above and choose the same parameters: the viscosity constant $\nu = 0.05$ and $N = 50$ implying $h = 0.02$. For this experiment, we take the Taylor-Green vortex which is given in our domain as

$$u(x_1, x_2, t) = (-U_0 \sin(2\pi x_1) \cos(2\pi x_2) e^{-2\nu t}, U_0 \cos(2\pi x_1) \sin(2\pi x_2) e^{-2\nu t}) \quad (7.2)$$

The initial vorticity is therefore taken as $\omega_0(x_1, x_2) = -U_0 4\pi \sin(2\pi x_1) \sin(2\pi x_2)$ with $U_0 = \frac{1}{2\pi}$.

We again perform the simulation for $N_{steps} = 100$ iterations with the total time $T = 1$. The plots for the approximated flow are given in Figure 7.5 — see the first row for the approximated solution at $t = 0.01, 0.5$ and 1 against the true flow in the second row. We also print the heatmap for the absolute l2-error of the solution. Notice that the approximated solution matches the true Taylor–Green vortex closely, however, the average relative error in this experiment is $E_{[0,T]} \approx 0.1270$ compared to $E_{[0,T]} \approx 0.0142$ in the previous one. As the error at $t = 0.01$ (see Figure 7.5) is concentrated along the boundary, this suggests that the error might be further improved by enforcing periodicity of the vorticity ω^θ as discussed in Remark 5.

Numerical Experiment 3 [Channel flow]. In this experiment we consider the periodic channel, which is represented by the box domain $D = [-H, H] \times [0, H]$ with boundary $\partial D = [-H, H] \times \{0\} \cup [-H, H] \times \{H\}$. We take similarly a uniform lattice $\Lambda = \{(i_1 - N)h, i_2 h : 0 \leq i_1 \leq 2N, 0 \leq i_2 \leq N\}$ with $H = 6$ and $N = 100$ implying $h = 0.06$. The vorticity is initialised as

$$\omega_0(x_1, x_2) = W_0 \cos\left(\frac{\pi}{3} x_2\right) \quad (7.3)$$

with $W_0 = 5$; the vorticity constant $\nu = 0.01$ and the boundary cutoff $\varepsilon = 0.3$.

The results of this simulation are presented in Figure 7.6 which includes the approximated streamlines and the vorticity of the flow for $t = 0.01, 0.33, 0.67$ and 1 .

Algorithm implementation details. Our implementation of the proposed algorithm is realized in Pytorch [26]. At every iteration of the algorithm, we train a NN which represents the vorticity ω^θ . The architecture used in our simulations is a fully connected feedforward NN with 4 hidden layers of dimension 512, i.e. with the structure $(2, 512, 512, 512, 512, 1)$. We use the ReLU activation function after all hidden layers.

At every step, we initialize a NN with the described architecture. For the initial weights, we use the default Pytorch initialization, i.e. uniform weights, and the optimization of the parameters is done with Adam [21]. For each iteration, the model is trained for 500 epochs. However, we observe that in general the loss function values are stabilized before 100 epochs, see Figure 7.1 for the loss function values for the first 200 epochs for the wall-bounded flow from Experiment 1.

To solve the Poisson equation, we use a Finite Element Method (FEM) for bounded domains (with Dirichlet or periodic boundary conditions). While a particular strength of our algorithm is that the Poisson solver can be used as a blackbox, allowing to employ the vast libraries of FEM software/toolboxes available, we instead used some simple custom made solvers working with uniform meshes on two-dimensional squares. In particular we did not consider more advanced algorithmic concepts such as adaptive mesh refinements.

Remark 6. *While the uniform meshing we used can certainly be inefficient and lead to suboptimal usage of computational resources by the FEM, it should be noted that it allows for rapid evaluation of the interpolation of the computed gridbased values, which is important for fast simulation of the random vortex dynamics (2.2), and thus for training the network ω^θ .*

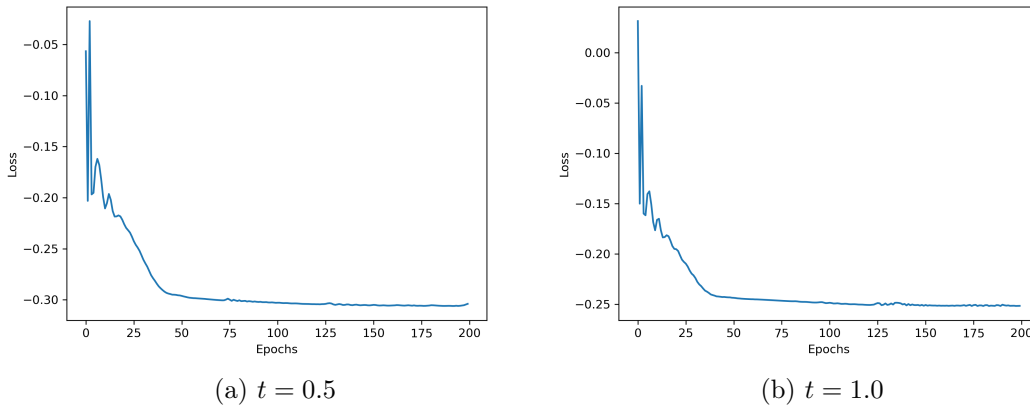


Figure 7.1: The loss function at different times t .

Also notice that as in our implementation we use only simple fully-connected NNs and initialize them at every iteration, one potential way to upgrade the algorithm is to improve the NN architecture. For instance, one can include the time dependence into the NN and try to incorporate the Markovian structure, e.g. using some attention mechanism.

Acknowledgements/Funding

Vladislav Cherepanov is fully supported by the EPSRC Centre for Doctoral Training in Mathematics of Random Systems: Analysis, Modelling and Simulation (EP/S023925/1).

Sebastian W. Ertel has been supported by Deutsche Forschungsgemeinschaft (DFG) - Project-ID 318763901 - SFB1294 and by Deutsche Forschungsgemeinschaft (DFG) - Project-ID 410208580 - IRTG2544 ('Stochastic Analysis in Interaction').

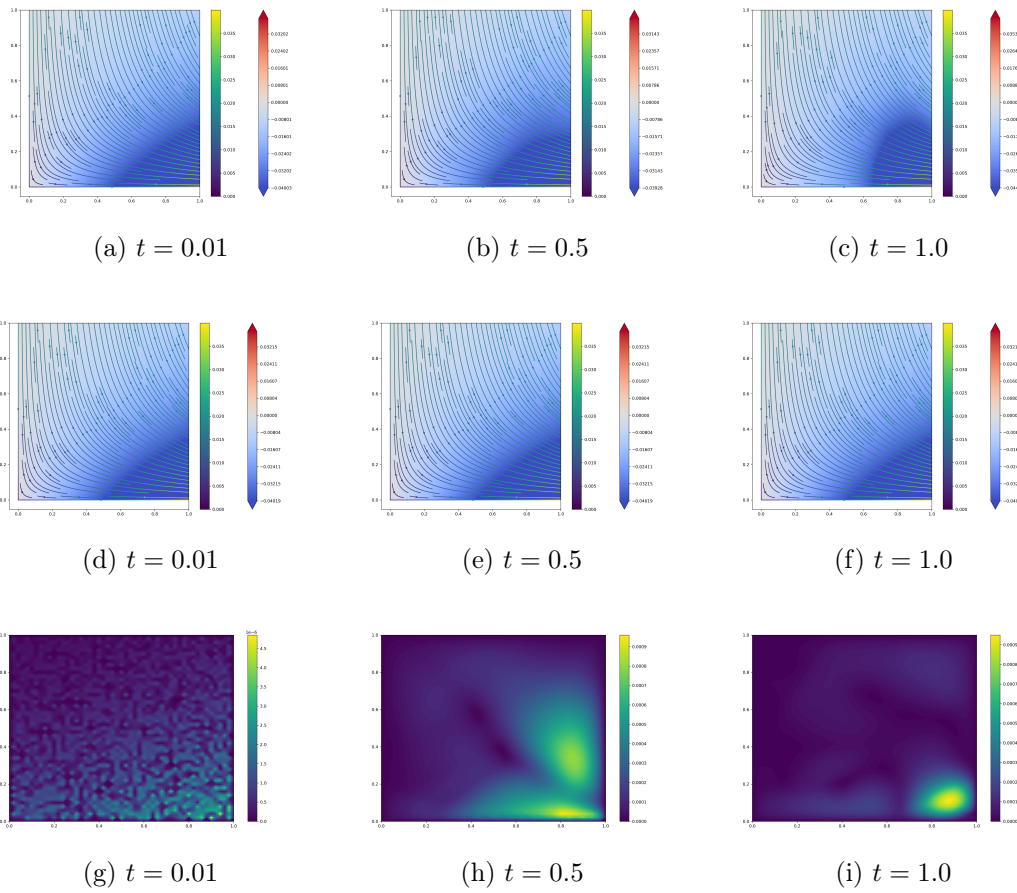


Figure 7.2: The fully-bounded flow (7.1): the first row represents the approximation at different times t ; the second row contains the true solution at the times; the third row represents the absolute l_2 -error of the approximation.

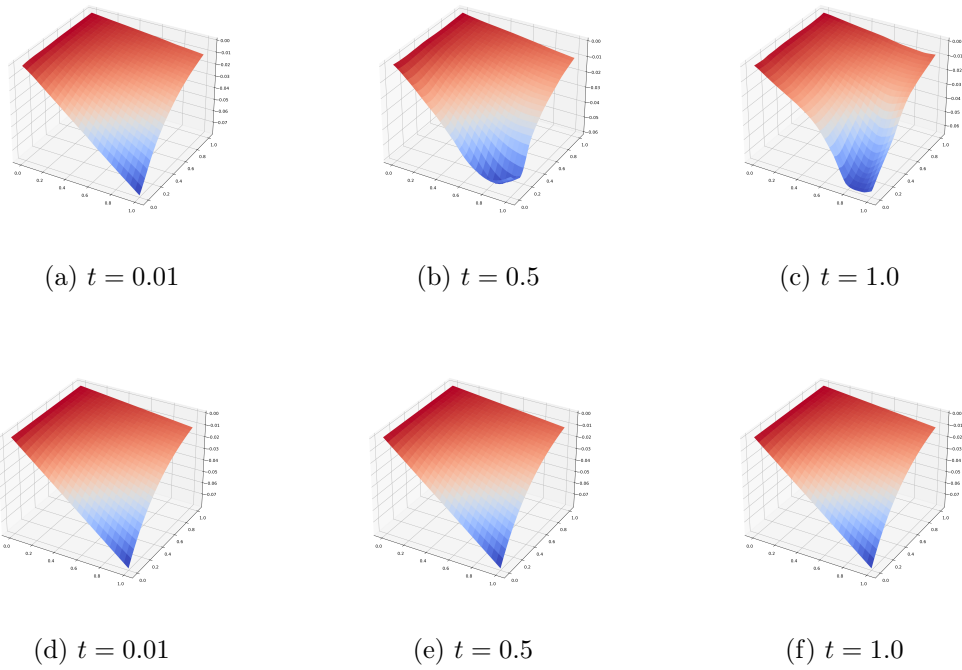


Figure 7.3: The fully-bounded flow (7.1): the first row contains the vorticity learned at different times t ; the second represents the true vorticity at the times.

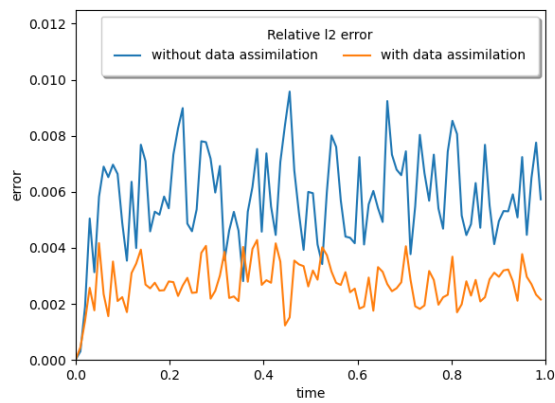


Figure 7.4: The relative l2 error with and without data assimilation as function of time t .

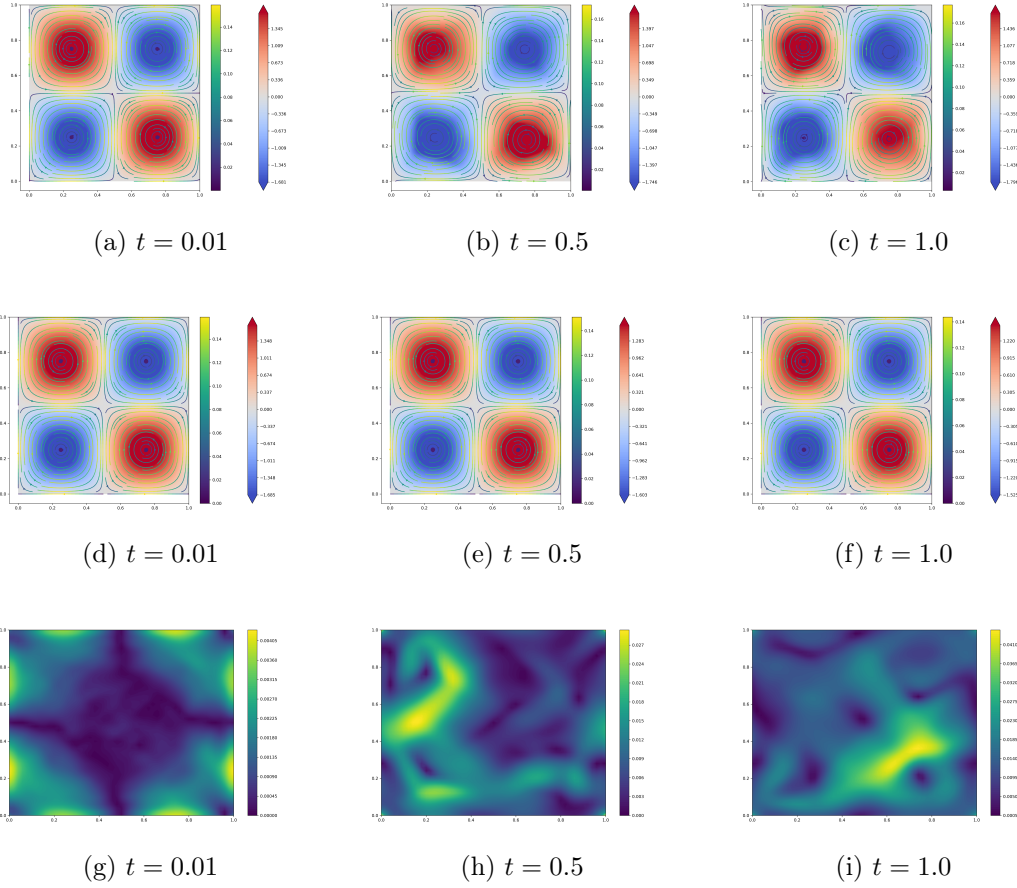


Figure 7.5: The fully-periodic flow (7.2) (Taylor–Green vortex): in the first and second row there are the approximation and the true solution at different times t ; in the third row, the absolute l2-error of the approximation is printed.

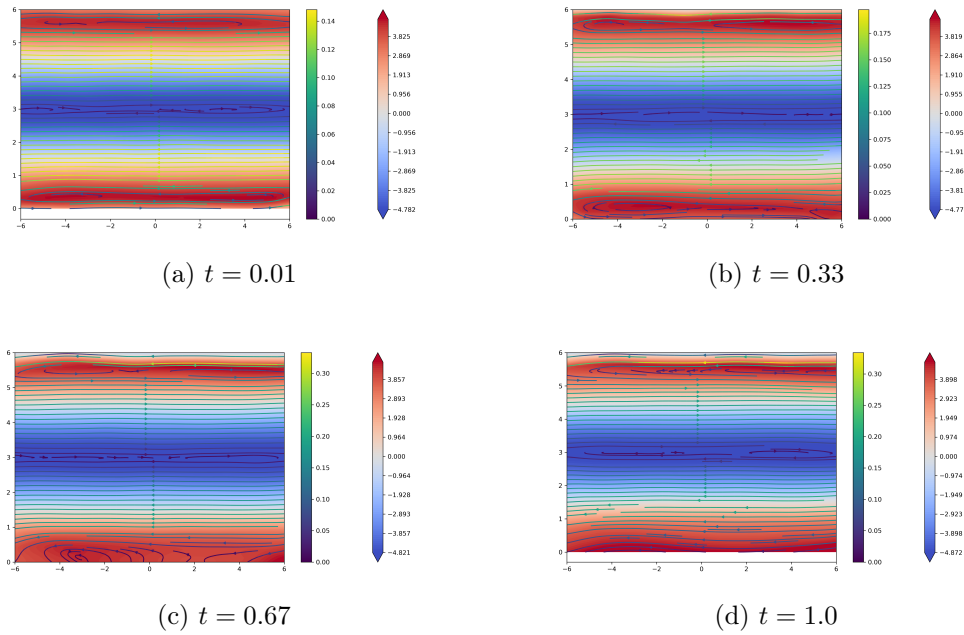


Figure 7.6: The periodic channel (7.3): the approximated flow for different times t .

Bibliography

- [1] Anderson C., Greengard C. On vortex methods. In *SIAM J. Numer. Anal.* **22** (3), 413-440, 1985.
- [2] Bai S., Kolter Z., Koltun V. Deep Equilibrium Models. In *Advances in neural information processing systems*. 2019.
- [3] Beck C., Becker S., Grohs P., Jaafari N., Jentzen A. Solving the Kolmogorov PDE by Means of Deep Learning. In *Journal of Nonlinear Science* 29:1563-1619, 2019.
- [4] Beck C., E W., Jentzen A. Machine Learning Approximation Algorithms for High-Dimensional Fully Nonlinear Partial Differential Equations and Second-order Backward Stochastic Differential Equations. *Journal of Scientific Computing* 88:73, 2021.
- [5] Cai S., Mao Z., Wang Z., Yin M., Karniadakis G. E. Physics-informed neural networks (PINNs) for fluid mechanics: A review. In *Acta Mech. Sin.*, pages 1–12, 2022.
- [6] Cherepanov V., Ertel S., Qian Z., Wu J. Random vortex dynamics and Monte-Carlo simulations for wall-bounded viscous flows. In *arXiv: 2403.15549*, 2024.
- [7] Cherepanov, V., Liu, J.-G., Qian, Z. On the dynamics of the boundary vorticity for incompressible viscous flows. In *Journal of Scientific Computing*, 99(2), 2024.
- [8] Cherepanov V., Qian Z. Monte-Carlo method for incompressible fluid flows past obstacles. In *arXiv: 2304.09152*, 2023.
- [9] Chorin A. J. Numerical study of slightly viscous flow. In *J. Fluid Mech.* 57, 785–796, 1973.
- [10] Cottet G.-H. A vorticity creation algorithm for the Navier-Stokes equations in arbitrary domain. In *Navier-Stokes Equations and Related Nonlinear Problems* pp 335-349, 1995.
- [11] Evans L. C. Partial Differential Equations. In *AMS Graduate Studies in Mathematics*, Second Edition, 2010.
- [12] Evensen G., Vossepoel F., van Leeuwen P.-J. Data Assimilation Fundamentals - A Unified Formulation of the State and Parameter Estimation Problem. In *Springer Nature*, 2022.
- [13] Goodman, J. Convergence of the random vortex method. In *Comm. Pure Appl. Math.* **40**(2), 189-220, 1987.
- [14] Grohs P., Hornung F., Jentzen A., von Wurstemberger P. A proof that artificial neural networks overcome the curse of dimensionality in the numerical approximation of Black-Scholes partial differential equations. In *Memoirs of the American Mathematical Society* 284, 1-106, 2023.
- [15] Han J., E W., Jentzen A. Solving high-dimensional partial differential equations using deep learning. In *Proceedings of the National Academy of Sciences* 115 (34), 8505–8510.

- [16] Jin X., Cai S., Li H., Karniadakis G.E. NSFnets (Navier-Stokes flow nets): Physics-informed neural networks for the incompressible Navier-Stokes equations. In *J. Comput. Phys.* 426:109951, 2021.
- [17] Kashefi A., Mukerji T. Physics-informed PointNet: A deep learning solver for steady-state incompressible flows and thermal fields on multiple sets of irregular geometries. In *Journal of Computational Physics*, Volume 468, 2022.
- [18] Kashefi A., Mukerji T. Prediction of fluid flow in porous media by sparse observations and physics-informed PointNet. In *Neural Networks*, Volume 167, October 2023.
- [19] Kashefi A., Mukerji T. Physics-informed PointNet: On how many irregular geometries can it solve an inverse problem? Application to linear elasticity. In *Journal of Machine Learning for Modeling and Computing*, Volume 4, Issue 4, 2023.
- [20] Kim J., Lee K., Lee D., Jhin S. Y., Park N. DPM: A novel training method for physics-informed neural networks in extrapolation. In *Proceedings of the AAAI Conf. on Artificial Intelligence*, pages 8146–8154, 2021.
- [21] Kingma D. P., Ba J. Adam: A method for stochastic optimization. In *arXiv:1412.6980*, 2015.
- [22] Krishnapriyan A., Gholami A., Zhe S., Kirby R., Mahoney M. W. Characterizing possible failure modes in physics-informed neural networks. In *Adv. Neural Inf. Process. Syst.* 34:26548–26560, 2021.
- [23] Long, D. G. Convergence of the random vortex method in two dimensions. In *J. of Amer. Math. Soc.* 1(4), 779-804, 1988.
- [24] Majda, A. J., Bertozzi A. L. Vorticity and incompressible flow. In *Cambridge University Press*, 2002.
- [25] McConkey R., Yee E., Lien F.-S. Deep Structured Neural Networks for Turbulence Closure Modelling. In *Physics of Fluids* 34 (3), 2022.
- [26] Paszke A., Gross S., Massa F., Lerer A., Bradbury J., Chanan G., Killeen T., Lin Z., Gimelshein N., Antiga L., et al. Pytorch: An imperative style, high-performance deep learning library. Adv. In *Neural Inf. Process. Syst.*, 32, 2019.
- [27] Qian Z. Stochastic formulation of incompressible fluid flows in wall bounded regions. In *arXiv:2206.05198v1*, 2022.
- [28] Qian Z., Süli E., Zhang Y. Random vortex dynamics via functional stochastic differential equations. In *Proc. Roy. Soc. A*, Vol. 478 (2266), 2022.
- [29] Raissi M., Perdikaris P., Karniadakis G. E. Physics-informed neural networks: A deep learning framework for solving forward and inverse problems involving nonlinear partial differential equations. In *J. Comput. Phys.* 378:686–707, 2019.
- [30] Sirignano J., Spiliopoulos K. DGM: A deep learning algorithm for solving partial differential equations. In *Journal of Computational Physics* 375, 1339–1364, 2018.

- [31] Sun L., Wang J.-X. Physics-constrained Bayesian neural network for fluid flow reconstruction with sparse and noisy data. In *Theor. Appl. Mech. Lett.* 10(3):161–169, 2020.
- [32] Wang S., Teng Y., Perdikaris P. Understanding and mitigating gradient flow pathologies in physics-informed neural networks. In *SIAM J. Sci. Comput.* 43(5):A3055–A3081, 2021.
- [33] Zhang R., Hu P., Meng Q., Wang Y., Zhu R., Chen B., Ma Z., Liu T.-Y. DRVN (Deep Random Vortex Network): A new physics-informed machine learning method for simulating and inferring incompressible fluid flows. In *Physics of Fluids* 34(10), 2022.